Supporting Information

Selection Criteria for Electrical Double Layer Structure Regulators enabling Stable Zn Metal Anodes

Cong Huang[a], Xin Zhao[b], Yisu Hao[a], Yujie Yang[a], Yang Qian[a], Ge Chang[a], Yan Zhang[a], Qunli Tang[a]*, Aiping Hu[a], and Xiaohua Chen[a]*

[a]College of Materials Science and Engineering, Hunan Province Key Laboratory for Advanced Carbon Materials and Applied Technology, Hunan University, Changsha 410082, P. R. China

E−mail: xiaohuachen@hnu.edu.cn; tangqunli@hnu.edu.cn

[b]Tsinghua Shenzhen International Graduate School, Tsinghua University, Shenzhen, 518055, P. R. China

1. Experimental Section

Materials: $ZnSO_4 \cdot 7H_2O$ (AR), Na_2SO_4 (anhydrous, AR), methanol (anhydrous, AR), ethanol (anhydrous, AR), 2-propanol (AR), dimethyl sulfoxide (AR), acetone (AR), N-methylpyrrolidone (AR), N,N-dimethylformamide (AR), 1,3-dioxolane (AR), and ethylene glycol (AR) were purchased from Sinopharm. Dimethyl carbonate (99%), glycerol (99%), 1,2-dimethoxyethane (99.5%), bis(2-methoxy ethyl)ether (99.5%), ethylene carbonate (>99%), propylene carbonate (99%), and $Zn(CH_3COO)_2 \cdot 2H_2O$ (AR) were purchased from Macklin. Sulfolane (>99%) was purchased from Aladdin.

Electrolyte preparation: 2M $ZnSO_4$ electrolyte was prepared by dissolving Zn salts ($ZnSO_4 \cdot 7H_2O$) in deionized water. The control electrolytes were prepared by adding solvents with different volume ratios (0.1 vol%, 0.5 vol%, and 1 vol%) into 80 mL 2M $ZnSO_4$ electrolyte. For sulfolane solvent, 100, 400, and 800 μL sulfolane were added into 80 mL 2M $ZnSO_4$ electrolyte, respectively. The optimization concentration for sulfolane was 0.5 vol%, and the corresponding electrolyte was denoted as Sul/$ZnSO_4$. The preparation process of other control electrolytes was similar to that of electrolytes containing sulfolane except for adding different solvents.

Materials Characterization: The ionic conductivity of different electrolytes was measured using a conductivity meter (DDSF-308F). The Zn deposition morphology was acquired by the field-emission scanning electron microscopy (FESEM, Hitachi S-4800). A 3D measuring laser microscope (Olympus LEXT OLS4100) was operated to achieve the laser confocal scanning microscopy (LCSM) images of the Ti foils cycled in Sul/$ZnSO_4$ and $ZnSO_4$ electrolytes. The surface compositions of Zn anodes were investigated by X-ray photoelectron spectroscopy (XPS, ESCALAB 250Xi) equipped with Al Ka X-ray source. The Raman spectra were collected by HORIBA JY LabRAM HR Evolution. The SHIMADZU UV 2550 was adopted to record the concentration change of sulfolane additives during cycling.

Electrochemical Characterization: Tafel plots were measured by scanning between −0.8 and −1.1 V at 1 mV s^{-1} with Zn plate as the working electrode, Pt foil as the counter electrode, and Ag/AgCl as the reference electrode, respectively. The potentiostatic current-time transient curves were measured at a fixed potential of −1.1 V in $ZnSO_4$ electrolyte using three-electrode system. The hydrogen evolution reaction potential was recorded using linear sweep voltammetry method with a scan rate of 2 mV s^{-1} in 0.5M Na_2SO_4 electrolyte. In the alternating current voltammetry tests, the frequency is 6 Hz and the amplitude (A) is 5 mV, with a potential range extended from 0.9 to 0.1 V versus Zn^{2+}/Zn. The selective region of phase angles was 0 and 90°. Zn symmetric cells (ZBs) were assembled by sandwiching the glass fiber (separators) between commercial Zn plates (100 μm, 58.5 mAh cm^{-2}) in CR2032-type cell filled with different electrolytes. Zn|Cu half cells were assembled using Zn plate (100 μm, 58.5 mAh cm^{-2}) as anode, Cu foils (20 μm) as cathodes, glass fiber as separator. The V_2O_5 and MnO_2 electrodes were prepared by casting slurry onto a carbon cloth (HESEN, HCP330N). The slurry was composed of commercial V_2O_5 (Sigma-Aldrich) or MnO_2 (Saibo materials), conductive carbon (Ketjen Black) and PVDF binder (Kejing, Shenzhen) with mass ratio of 7:2:1. The V_2O_5 and MnO_2 electrode was then dried in an oven under 80 ℃ for 12 h. The mass loading of V_2O_5 and MnO_2 electrodes is 5.2 ± 0.2 and 8.4 ± 0.4 mg cm^{-2}, respectively. Zn metal full cells were assembled using Zn plate (10 μm, 5.85 mAh cm^{-2}) and glass fiber as the anode and separator, respectively. For Zn-V_2O_5 cells, V_2O_5 electrodes were employed as cathodes, and Sul/$ZnSO_4$ and $ZnSO_4$ solution as electrolytes. For Zn-MnO_2 cells, 0.1M $MnSO_4$ were introduced into Sul/$ZnSO_4$ and $ZnSO_4$ electrolytes for inhibiting the dissolution of Mn^{2+}, and MnO_2 electrodes were employed as cathodes.

Computional methods: The adsorption energy calculations were performed using the Vienna ab-initio simulation package (VASP). The projector-augmented wave (PAW) method was used to represent the core-valence interaction.[S1] The plane wave energy cutoff was set to 450 eV. The generalized gradient approximation (GGA) with the Perdew-Burke-Ernzerhof (PBE)

exchange-correlation functional[S2] were used in our calculations. The first Brillion zone k-point sampling utilizes the Monkhorst-Pack scheme with a 2 × 2 × 1 grid meshes. The energy and force criterion for convergence of the electron density are set at 10^{-6} eV and 0.05 eV/Å, respectively. The long-range dispersion (van der Waals interactions) corrections were evaluated using DFT-D3 method.[S3] A 5×5 supercell with five-layer thickness for Zn (0001) surface is adopted which contains 125 Zn atoms. The bottom two layers are fixed during structure optimization. A vacuum gap of approximately 12 Å was used in normal direction to avoid the interaction between slabs. The adsorption energy (E_{ads}) of molecules is calculated according to the following equation: $E_{ads} = E_{tot}–E_{Zn}–E_{mol}$, where E_{tot}, E_{Zn} and E_{mol} are the total energy of surface with the adsorbed molecules, the energy of Zn surface and the molecule energy, respectively.

The HOMO-LUMO energy level calculations were performed via the Gaussian 16 suite of programs.[S4] The structures of the studied compounds were fully optimized at the B3LYP/6-311+G(d,p) level of theory. The vibrational frequencies of the optimized structures were carried out at the same level. The structures were characterized as a local energy minimum on the potential energy surface by verifying that all the vibrational frequencies were real. The energy of the HOMOs and LUMOs as well as their gaps were calculated. The Visual Molecular Dynamics (VMD) program[S5] was used to plot the color-filled isosurfaces graphs to visualize the molecular orbitals.

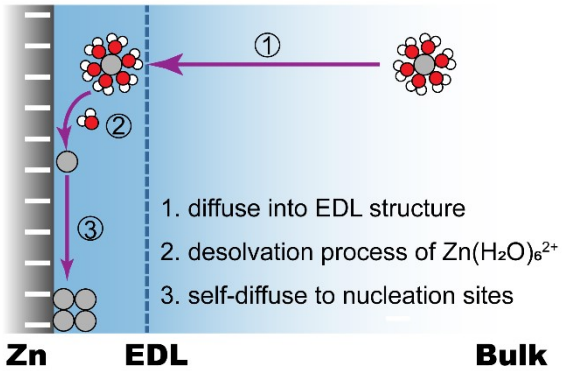

Fig. S1. Schematic of the Zn deposition process in the EDL structure.

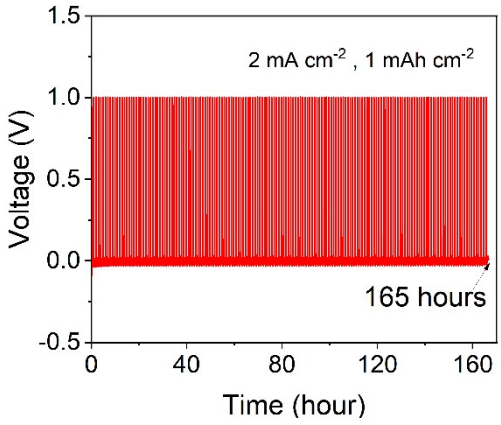

Fig. S2. Voltage profiles of Zn|Cu half cells using bare $ZnSO_4$ electrolytes.

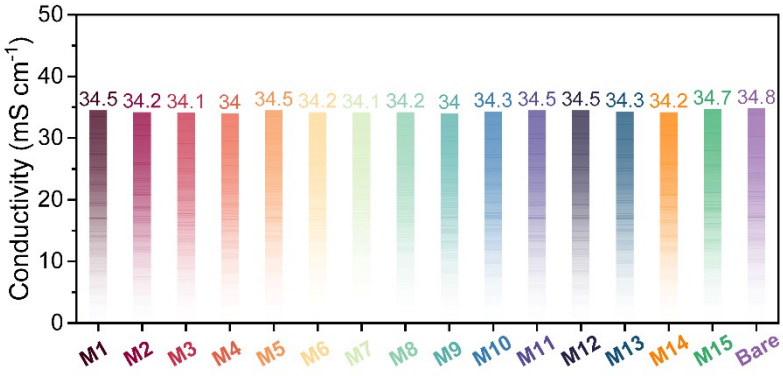

Fig. S3. Ion conductivity of selected representative electrolytes.

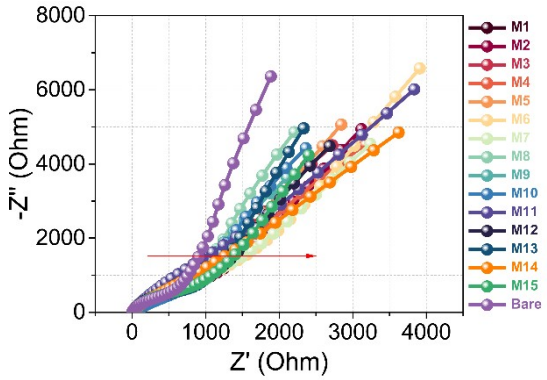

Fig. S4. EIS spectra of Zn|Cu half cells using selected representative electrolytes.

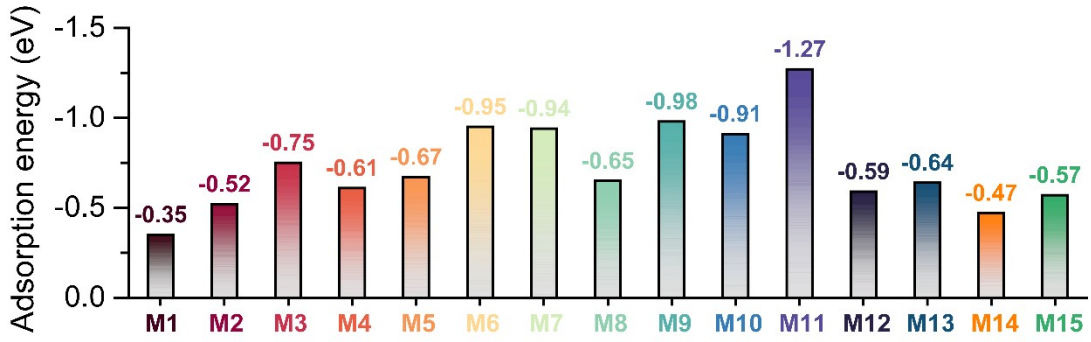

Fig. S5. Adsorption energy of solvent additives on the Zn (0001) surface.

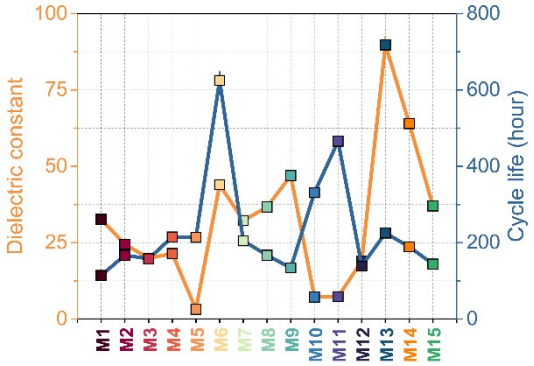

Fig. S6. Correlation between the cycle life of Zn|Cu half cells and dielectric constant of solvent additives.

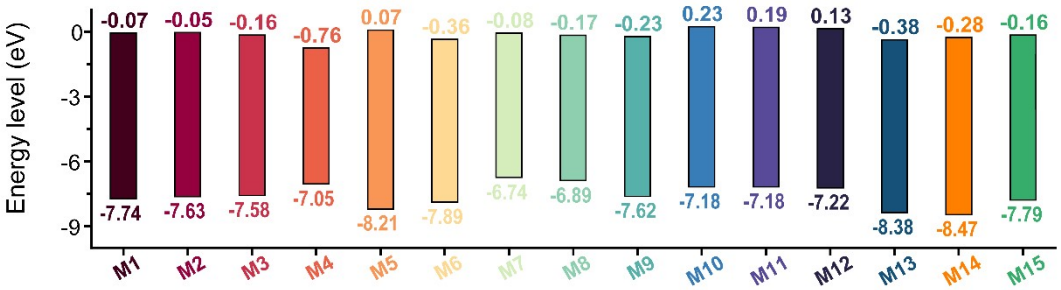

Fig. S7. HOMO-LUMO energy level of solvent additives.

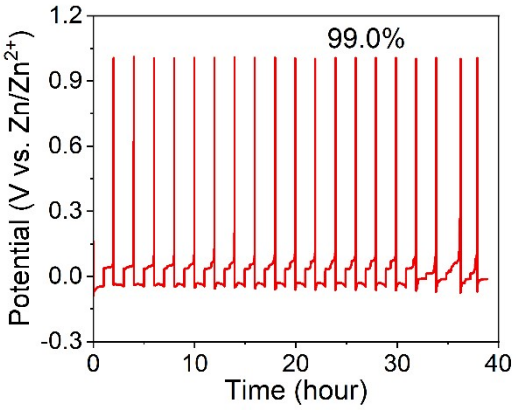

Fig. S8. Voltage profiles of Zn|Cu half cells using bare $ZnSO_4$ electrolytes at a current density of 10 mA cm^{-2} and a capacity of 10 mAh cm^{-2}.

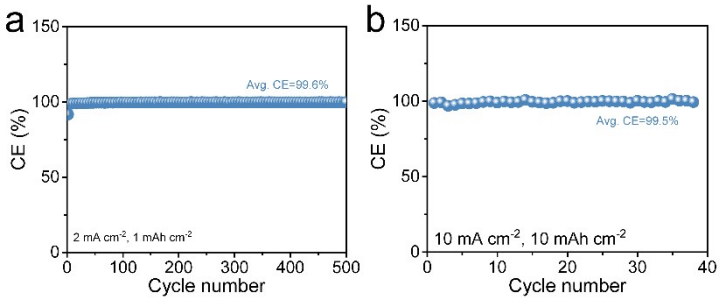

Fig. S9. CE of Zn|Cu half cells using 1 vol% DMSO at a current density of a) 2 mA cm^{-2} and b) 10 mA cm^{-2}.

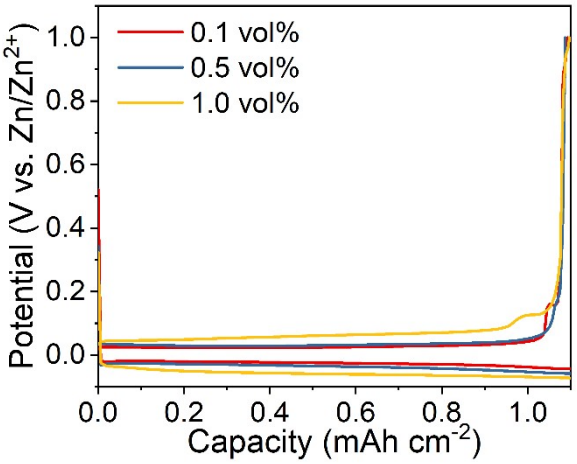

Fig. S10. Voltage profiles of Zn|Cu half cells using different concentration of sulfolane.

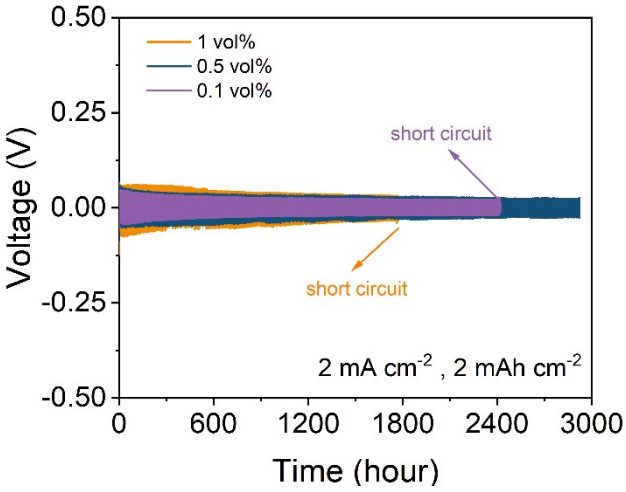

Fig. S11. Voltage profiles of Zn|Zn symmetric cells using different concentration of sulfolane.

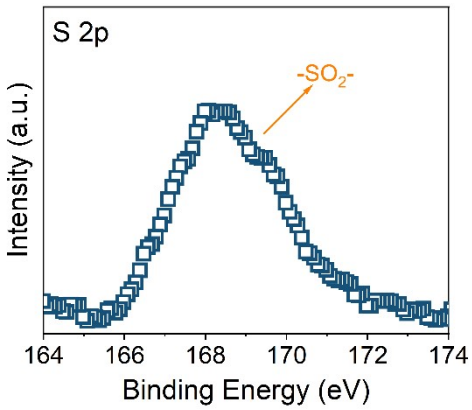

Fig. S12 The S 2p spectra of the Zn anode immersed in deionized water with 0.5 vol% sulfolane.

Table S1. The corrosion current density of Zn anodes in Sul/$ZnSO_4$ and $ZnSO_4$ electrolyte.

Electrolytes	Corrosion potential	Corrosion current density
$ZnSO_4$	−0.973 V	0.74 mA cm^{-2}
Sul/$ZnSO_4$	−0.97 V	0.12 mA cm^{-2}

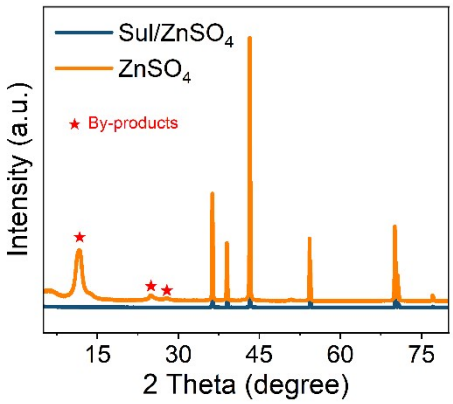

Fig. S13 The XRD pattern of Zn anodes immersed in Sul/$ZnSO_4$ and $ZnSO_4$ electrolytes.

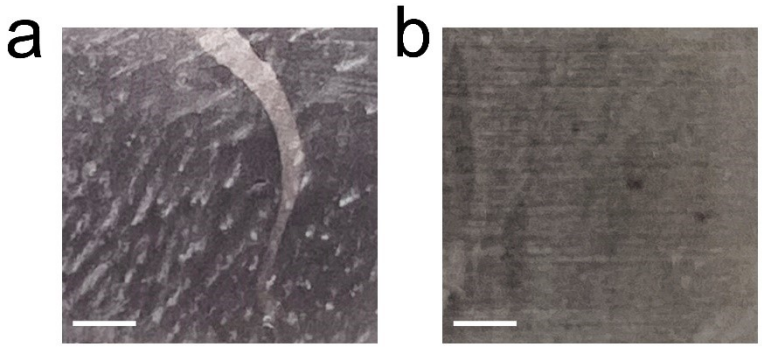

Fig. S14. Optical photos of Cu foils after tested at a current density of 2 mA cm^{-2} for 100 s in a) $ZnSO_4$ and b) Sul/$ZnSO_4$ electrolytes (Scale bar: 200 mm).

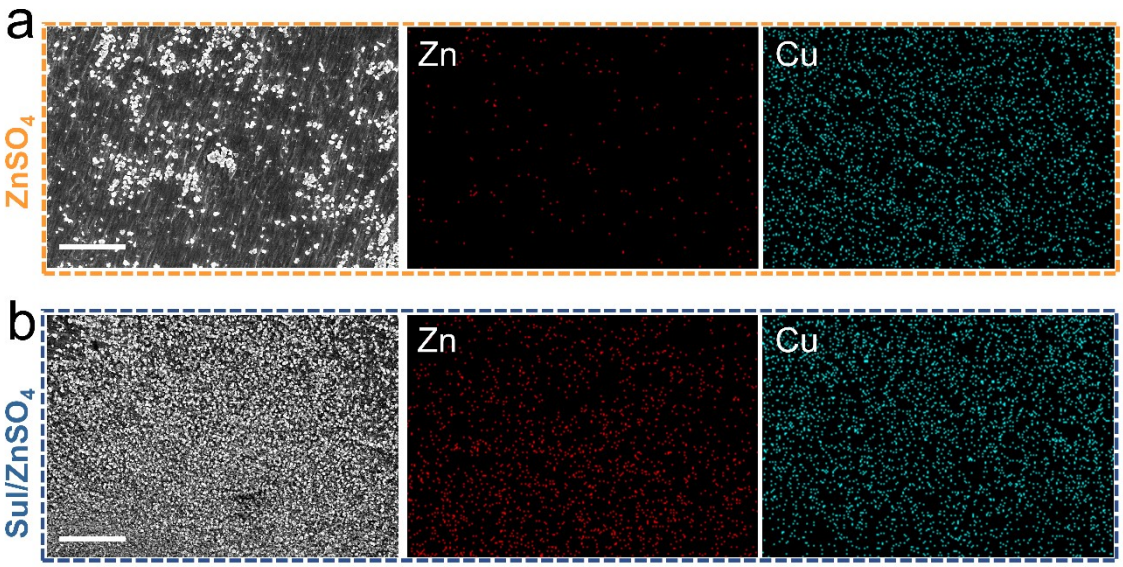

Fig. S15. SEM images and EDS mapping of Cu foils after tested at a current density of 2 mA cm^{-2} for 100 s in a) $ZnSO_4$ and b) Sul/$ZnSO_4$ electrolytes (Scale bar: 25 μm).

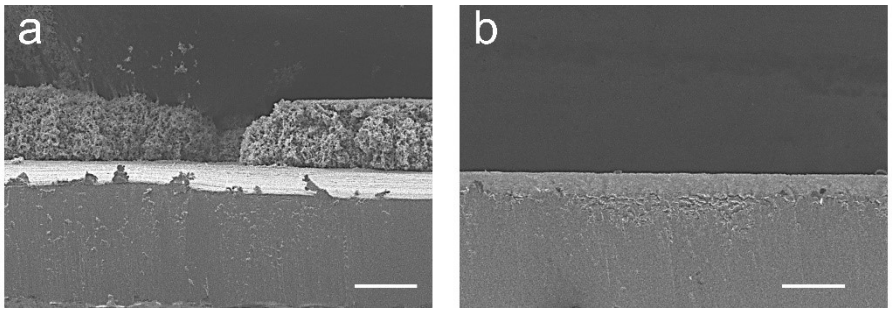

Fig. S16 Cross-sectional SEM images of Cu cathodes tested in a) $ZnSO_4$ electrolytes and b) Sul/ $ZnSO_4$ electrolytes (Scale bar: 50 μm).

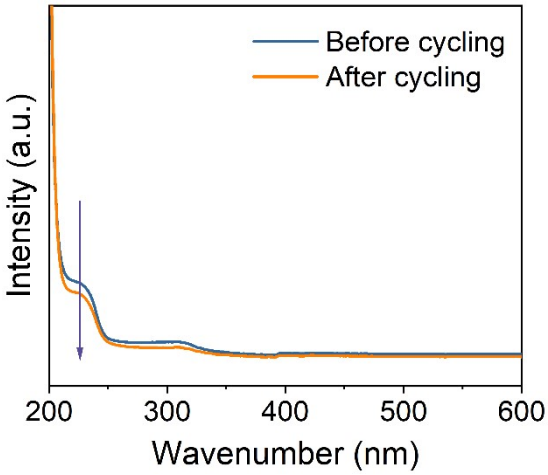

Fig. S17. UV-vis spectra of Sul/$ZnSO_4$ electrolytes before and after cycling.

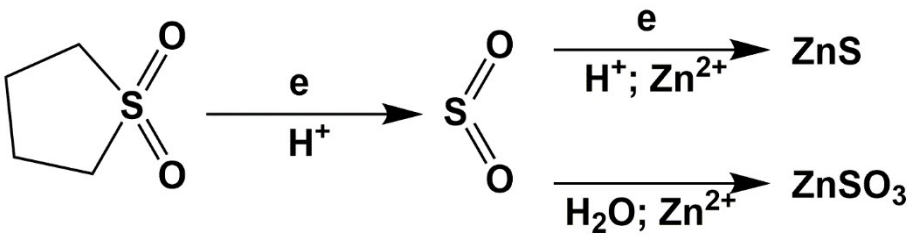

Fig. S18. The possible decomposition pathway of sulfolane during cycling.

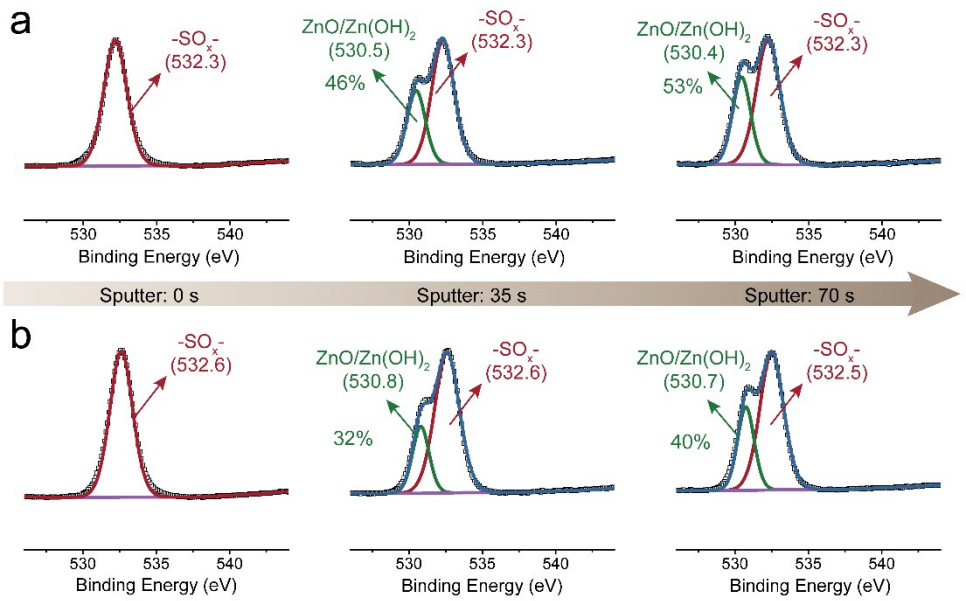

Fig. S19. XPS depth profiles of O 1s spectra of Zn anodes cycled in a) Sul/$ZnSO_4$ electrolytes and b) $ZnSO_4$ electrolytes (x=2, 3, or 4).

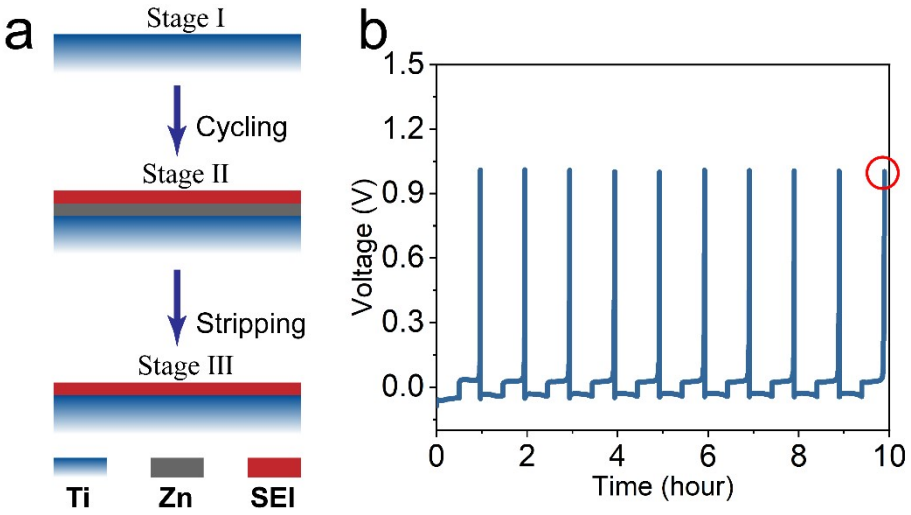

Fig. S20. a) Schematic of SEI formation process on the Ti foil. b) Voltage profiles of Zn|Ti half cells at 2 mA cm^{-2} with a capacity of 1 mAh cm^{-2}.

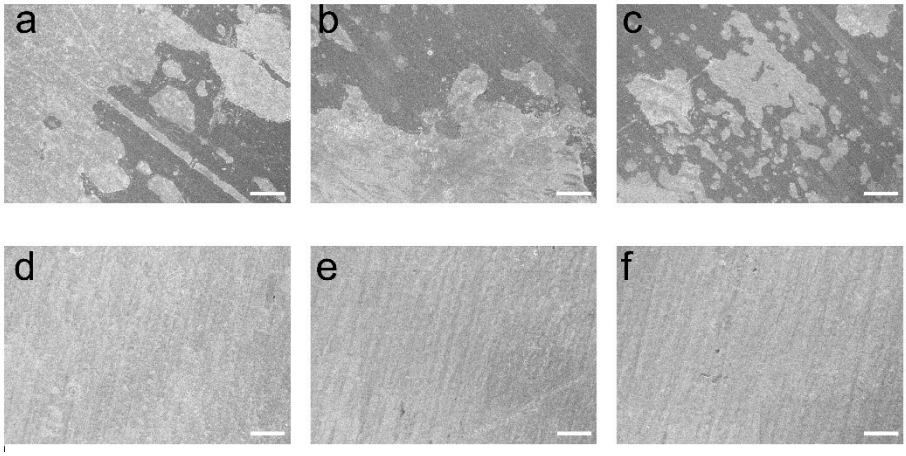

Fig. S21. SEM images of the SEI layer formed in a-c) $ZnSO_4$ and d-f) Sul/$ZnSO_4$ electrolytes (Scale bar: 50 μm).

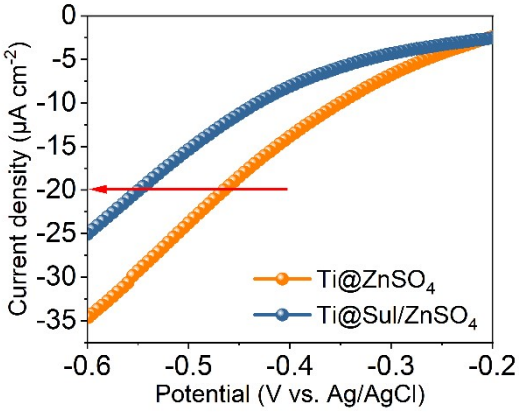

Fig. S22. LSV curves of Ti@Sul/$ZnSO_4$ and Ti@/$ZnSO_4$ in 0.5M Na_2SO_4 electrolytes at a scan rate of 2 mV s^{-1}.

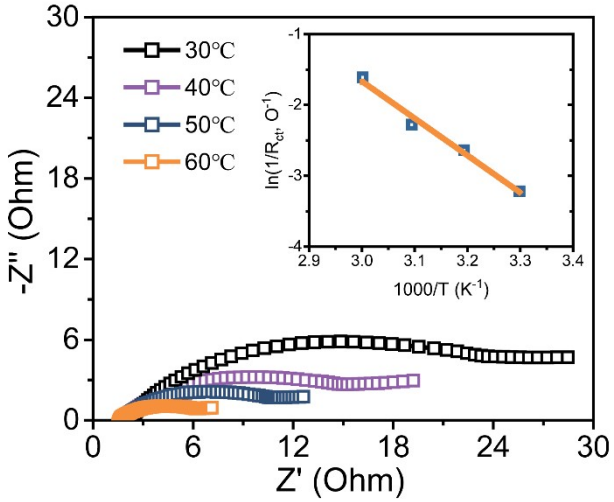

Fig. S23. EIS spectra of Zn|Zn symmetric cells in Sul/$ZnSO_4$ electrolytes under different temperature.

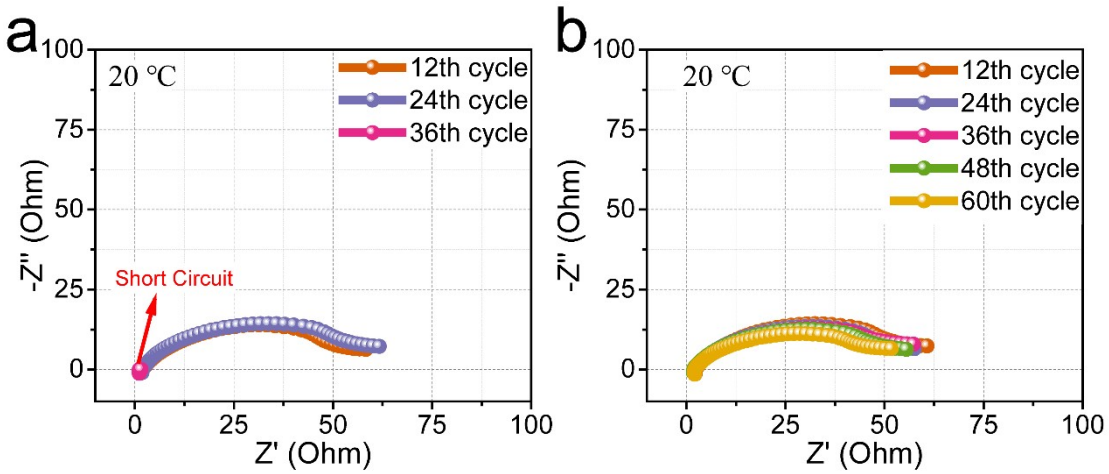

Fig. S24. EIS spectra of Zn|Zn symmetric cells in a) $ZnSO_4$ and b) Sul/$ZnSO_4$ electrolytes at different cycles.

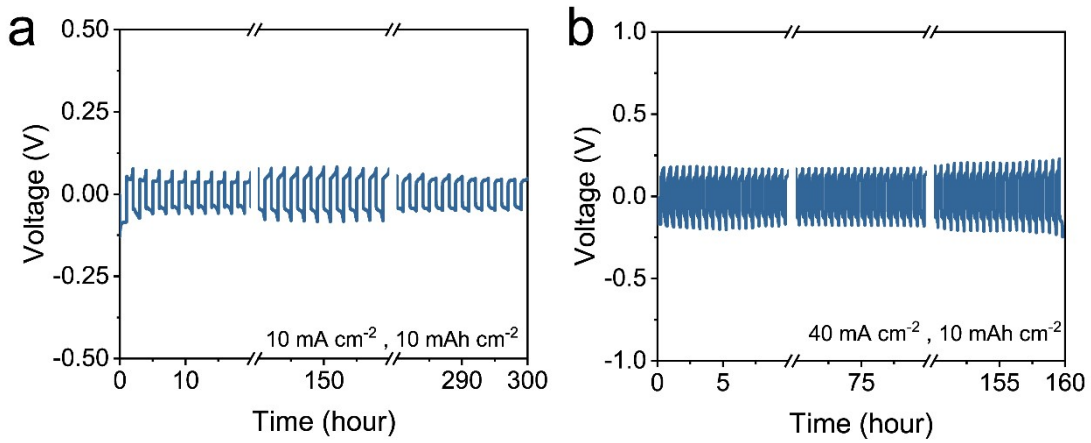

Fig. S25. Enlarged voltage profiles of of Zn|Zn symmetric cells in Sul/$ZnSO_4$ electrolytes at a) 10 mA cm^{-2} with 10 mAh cm^{-2} and b) 40 mA cm^{-2} with 10 mAh cm^{-2}.

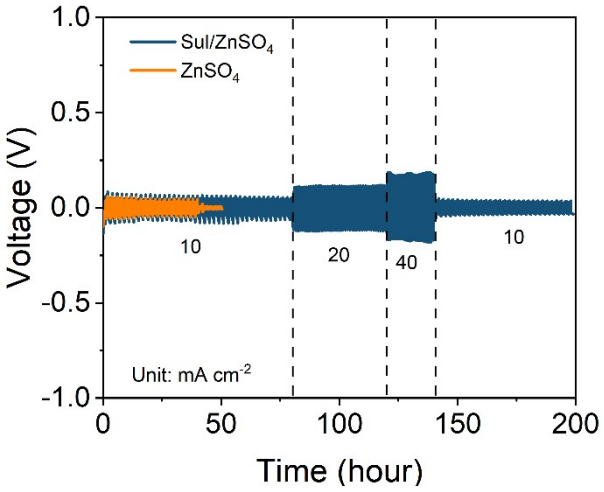

Fig. S26. Rate performance of Zn|Zn symmetric cells in Sul/$ZnSO_4$ electrolytes.

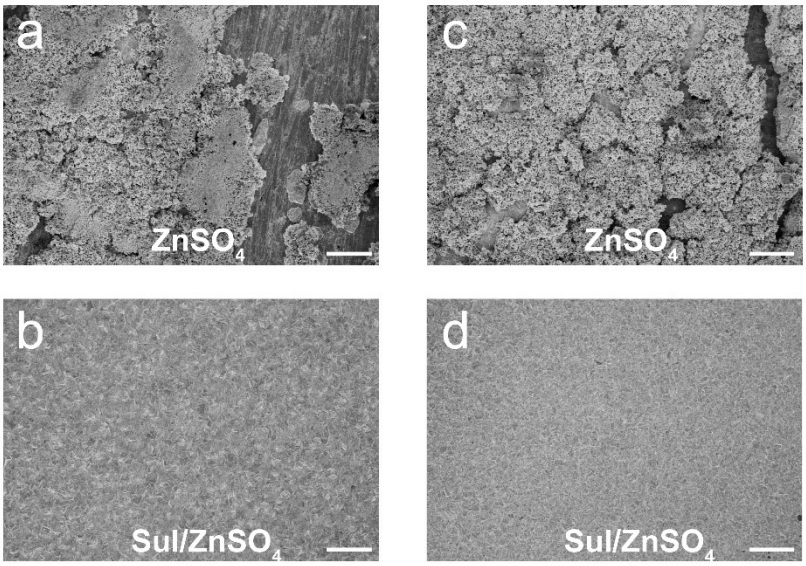

Fig. S27. SEM images of Zn anodes cycled at a-b)10 mA cm^{-2} with 10 mAh cm^{-2} and c-d)40 mA cm^{-2} with 10 mAh cm^{-2} (Scale bar: 50 μm).

Table S2. The performance comparison of Zn|Cu half cells in SA/$ZnSO_4$ electrolytes with other reported works.

Solvent	Capacity (mAh cm^{-2})	Current density (mA cm^{-2})	CPC (mAh cm^{-2})	Volume Ratio	Ref.
Sulfolane	**10**	**40**	**3200**	**0.5%**	**This work**
Ethylene glycol	1	2	145	40%	[S6]
Dimethyl sulfoxide	0.5	0.5	250	18.9%	[S7]
Propylene carbonate	0.5	10	1000	50%	[S8]
N-methyl-2-pyrrolidone	5	5	488	5%	[S9]
N, N-dimethyl acetamide	3	3	1500	10%	[S10]
1,2-dimethoxyethane	2.5	5	2750	40%	[S11]
Diethyl ether	0.2	0.2	50	2%	[S12]
N,N-dimethylformamide	0.5	0.5	500	30%	[S13]
1,3-dioxolane	1	1	490	50%	[S14]
Glycerol	2	6	900	50%	[S15]
1,2-dimethoxyethane	2	2	380	1%	[S16]
ethylene glycol	0.5	5	2000	68%	[S17]
N-methyl-2-pyrrolidone	10	5	500	5%	[S18]

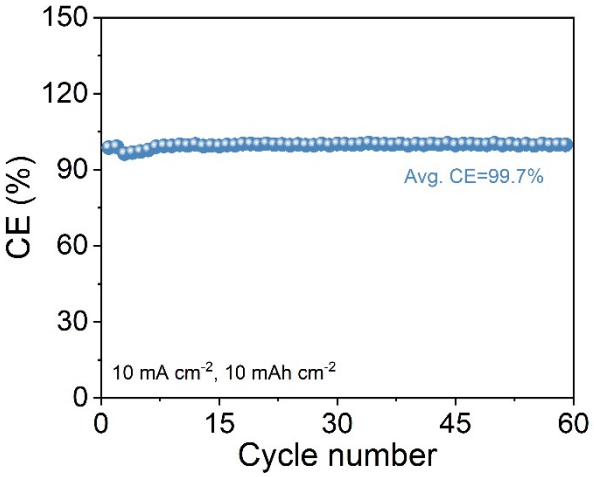

Fig. S28. CE evolution of Zn|Cu half cells using aged Sul/$ZnSO_4$ electrolytes.

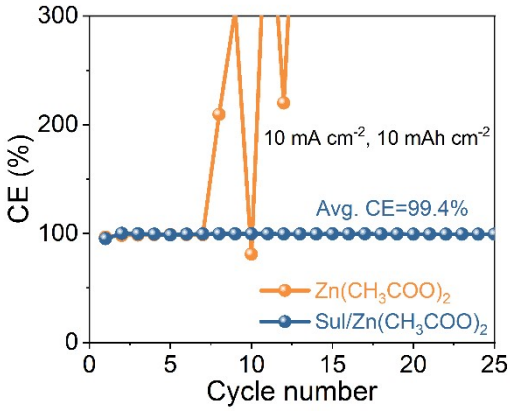

Fig. S29. CE evolution of Zn|Cu half cells using Sul/$Zn(CH_3COO)_2$ and $Zn(CH_3COO)_2$ electrolytes

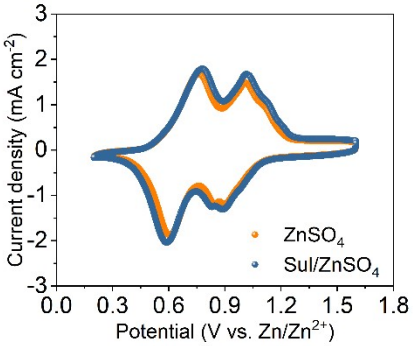

Fig. S30. CV curves of Zn-V_2O_5 full cells in Sul/$ZnSO_4$ and $ZnSO_4$ electrolytes at a scan rate of 0.3 mV s^{-1}.

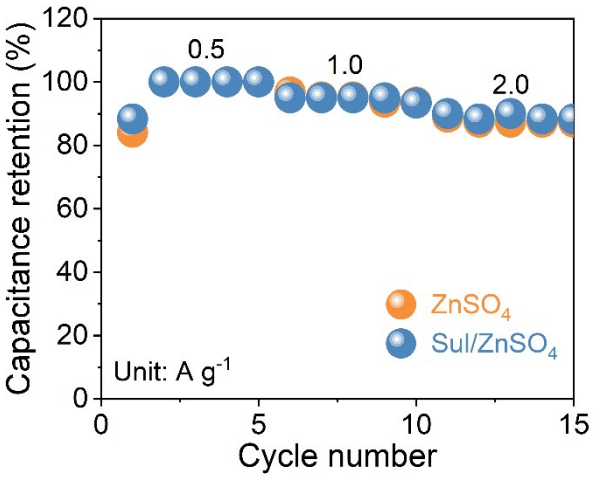

Fig. S31. Rate performance of Zn-V_2O_5 full cells in Sul/$ZnSO_4$ and $ZnSO_4$ electrolytes.

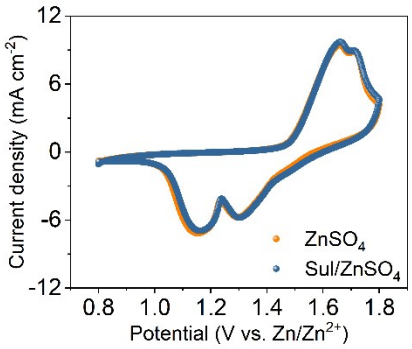

Fig. S32. CV curves of Zn-MnO_2 full cells in Sul/$ZnSO_4$ and $ZnSO_4$ electrolytes at a scan rate of 0.5 mV s^{-1}

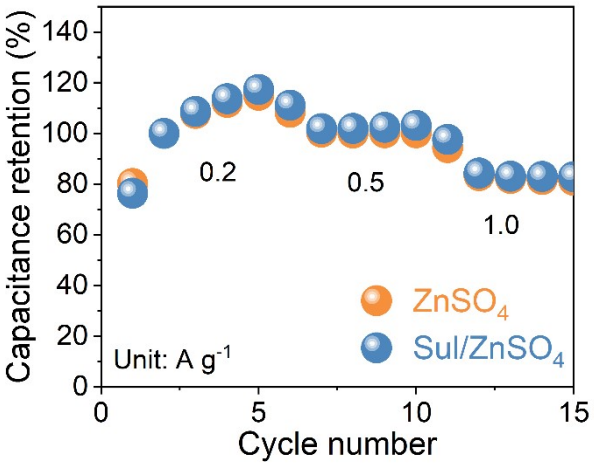

Fig. S33. Rate performance of Zn-MnO_2 full cells in Sul/$ZnSO_4$ and $ZnSO_4$ electrolytes.

Reference

[S1] a) P. E. Blöchl, Phys. Rev. B: Condens. Matter Mater. Phys. **1994**, 50, 17953; b) G. Kresse, D. Joubert, Phys. Rev. B: Condens. Matter Mater. Phys. **1999**, 59, 1758.

[S2] J. P. Perdew, K. Burke, M. Ernzerhof, Phys. Rev. Lett. **1996**, 77, 3865.

[S3] S. Grimme, J. Antony, S. Ehrlich, H. Krieg, J. Chem. Phys. **2010**, 132, 154104.

[S4] M. J. Frisch, G. W. Trucks, H. B. Schlegel, et al., Gaussian 16 Revision. A.03, Gaussian Inc., Wallingford, CT, 2016.

[S5] W. Humphrey, A. Dalke and K. Schulten, J Mol Graph Model, **1996**, 14, 33-38.

[S6] N. N. Chang, T. Y. Li, R. Li, S. N. Wang, Y. B. Yin, H. M. Zhang, X. F. Li, Energy & Environmental Science **2020**, 13, 3527.

[S7] L. Cao, D. Li, E. Hu, J. Xu, T. Deng, L. Ma, Y. Wang, X. Q. Yang, C. Wang, J Am Chem Soc **2020**, 142, 21404.

[S8] F. Ming, Y. Zhu, G. Huang, A. H. Emwas, H. Liang, Y. Cui, H. N. Alshareef, J Am Chem Soc **2022**, 144, 7160.

[S9] T. C. Li, Y. Lim, X. L. Li, S. Z. Luo, C. J. Lin, D. L. Fang, S. W. Xia, Y. Wang, H. Y. Yang, Advanced Energy Materials **2022**, 12, 2103231.

[S10] W. Deng, Z. Xu, X. Wang, Energy Storage Materials **2022**, 52, 52.

[S11] G. Ma, L. Miao, Y. Dong, W. Yuan, X. Nie, S. Di, Y. Wang, L. Wang, N. Zhang, Energy Storage Materials **2022**, 47, 203.

[S12] W. N. Xu, K. N. Zhao, W. C. Huo, Y. Z. Wang, G. Yao, X. Gu, H. W. Cheng, L. Q. Mai, C. G. Hu, X. D. Wang, Nano Energy **2019**, 62, 275.

[S13] Y. Ma, Q. Zhang, L. Liu, Y. Li, H. Li, Z. Yan, J. Chen, Natl Sci Rev **2022**, 9, nwac051.

[S14] H. Du, K. Wang, T. Sun, J. Shi, X. Zhou, W. Cai, Z. Tao, Chemical Engineering Journal **2022**, 427.

[S15] Y. Zhang, M. Zhu, K. Wu, F. Yu, G. Wang, G. Xu, M. Wu, H.-K. Liu, S.-X. Dou, C. Wu, Journal of Materials Chemistry A **2021**, 9, 4253.

[S16] J. Cui, X. Liu, Y. Xie, K. Wu, Y. Wang, Y. Liu, J. Zhang, J. Yi, Y. Xia, Materials Today Energy **2020**, 18.

[S17] R. Z. Qin, Y. T. Wang, M. Z. Zhang, Y. Wang, S. X. Ding, A. Y. Song, H. C. Yi, L. Y. Yang, Y. L. Song, Y. H. Cui, J. Liu, Z. Q. Wang, S. N. Li, Q. H. Zhao, F. Pan, Nano Energy **2021**, 80, 105478.

[S18] D. Wang, D. Lv, H. Liu, S. Zhang, C. Wang, C. Wang, J. Yang, Y. Qian, Angew Chem Int Ed Engl **2022**, e202212839.